Muonic molecular ions $pp\mu$ and $pd\mu$ driven by superintense VUV laser pulses: Postexcitation muonic and nuclear oscillations and high-order harmonic generation

Guennaddi K. Paramonov and Peter Saalfrank
Institut für Chemie, Universität Potsdam, Karl-Liebknecht-Strasse 24-25, 14476 Potsdam-Golm, Germany

(Received 28 February 2018; published 17 May 2018)

The non-Born-Oppenheimer quantum dynamics of $pp\mu$ and $pd\mu$ molecular ions excited by ultrashort, superintense VUV laser pulses polarized along the molecular axis (z) is studied by the numerical solution of the time-dependent Schrödinger equation within a three-dimensional (3D) model, including the internuclear distance R and muon coordinates z and ρ, a transversal degree of freedom. It is shown that in both $pp\mu$ and $pd\mu$, muons approximately follow the applied laser field out of phase. After the end of the laser pulse, expectation values $\langle z\rangle$, $\langle\rho\rangle$, and $\langle R\rangle$ demonstrate "post-laser-pulse" oscillations in both $pp\mu$ and $pd\mu$. In the case of $pd\mu$, the post-laser-pulse oscillations of $\langle z\rangle$ and $\langle R\rangle$ appear as shaped "echo pulses." Power spectra, which are related to high-order harmonic generation (HHG), generated due to muonic and nuclear motion are calculated in the acceleration form. For $pd\mu$ it is found that there exists a unique characteristic frequency $\omega_{\rm osc}^{pd\mu}$ representing both frequencies of post-laser-pulse muonic oscillations and the frequency of nuclear vibrations, which manifest themselves by very sharp maxima in the corresponding power spectra of $pd\mu$. The homonuclear $pp\mu$ ion does not possess such a unique characteristic frequency. The "exact" dynamics and power, and HHG spectra of the 3D model are compared with a Born-Oppenheimer, fixed-nuclei model featuring interesting differences: postpulse oscillations are absent and HHG spectra are affected indirectly or directly by nuclear motion.

DOI: 10.1103/PhysRevA.97.053408

I. INTRODUCTION

Excitation of muonic atoms and molecular ions by very intense laser pulses continues to attract considerable attention [1–8]. While in muonic molecular ions the main emphasis is still made on the muon-catalyzed fusion [7,9], other laser-induced processes are also very interesting for other reasons.

In particular, power spectra of $p\mu$ and $d\mu$ muonic hydrogen isotopes calculated in Ref. [1] showed the possibility to generate harmonics of a very high order (more than 1200) when the atoms were excited by a single VUV laser pulse with a frequency $\hbar\omega_l = 59$ eV and a peak intensity of $I_0 = 1.05 \times 10^{23}$ W/cm^2. There, also the role of finite-mass and finite-size effects of the atomic nuclei was emphasized. Similar work was done in Ref. [3] on muonic hydrogenlike systems with increasing nuclear charge. Other phenomena addressed in the context of strongly laser-driven muonic atoms are the coherent excitation of nuclei [2] and zeptosecond pulse generation [4,5].

In Ref. [8], laser-pulse driven muonic *molecular ions* $dd\mu$ and $dt\mu$ were studied, including (along with laser-enhanced fusion) coherent post-laser-pulse muonic oscillations and high-order harmonic generation. For postlaser oscillations and the energy uptake from the field by the molecule, strong non-Born-Oppenheimer effects were found.

In the present work we address similar problems in muonic molecular ions $pp\mu$ and $pd\mu$ which are excited by a single VUV laser pulse similar to the one used in Ref. [1]. Due to the smaller nuclear masses, even stronger non-Born-Oppenheimer effects are to be expected than for $dd\mu$ and $dt\mu$. Further, HHG spectra and their dependence on nuclear motion are now analyzed in greater detail. In particular, besides HHG due to muonic degrees of freedom, which had been considered before, we also report indirect and direct contributions to HHG due to *nuclear* motion, with a special emphasis being made to the difference of power and HHG spectra of homonuclear $pp\mu$ and heteronuclear $pd\mu$ suggested by the concept of inversion symmetry for nuclear motion, similar to that applied previously to muonic motion in $dd\mu$ and $dt\mu$ [8]. On the other hand, in contrast to our previous work [8], the problem of laser-enhanced fusion is not addressed here due to a very small fusion rate [9].

More specifically, we study the non-Born-Oppenheimer quantum dynamics of $pp\mu$ and $pd\mu$ excited by a superintense laser field linearly polarized along the molecular (z) axis by means of the numerical solution of the time-dependent Schrödinger equation within a three-dimensional (3D) model, including the internuclear distance R and two muon coordinates, z and ρ. The muon-nucleus and nucleus-nucleus Coulombic interactions are treated, as in Ref. [1], by making use of a nuclear drop model, while the muon is treated as being pointlike. The models used in our simulations, equations of motion, and numerical techniques are described in the next section. In Sec. III, the laser-induced quantum dynamics and the post-laser-pulse free evolution of $pp\mu$ and $pd\mu$ are presented and compared to those obtained at a fixed internuclear distance R, which is often referred to as the Born-Oppenheimer approximation. Post-laser-pulse muonic and nuclear oscillations on a long time scale are discussed in Sec. IV. Section V is devoted to power spectra generated by muonic and nuclear degrees of freedom. The results obtained are summarized in the concluding section VI.

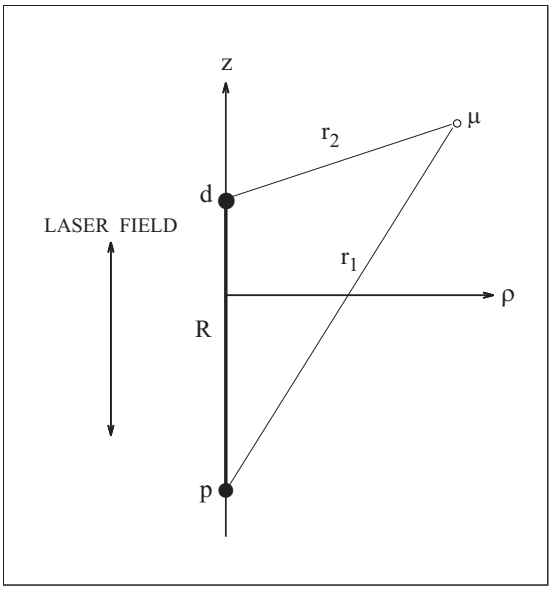

FIG. 1. Three-body 3D model of $pd\mu$ excited by the laser field linearly polarized along the z axis. The internuclear separation is R; the distances between the muon μ and each of the two nuclei, p and d, are r_1 and r_2, respectively. The coordinate z has its origin at the center of mass of the two nuclei.

II. MODELS, EQUATIONS OF MOTION, AND NUMERICAL TECHNIQUES

The three-body 3D model with the Coulombic interactions representing the $pd\mu$ molecular ion excited by a laser field linearly polarized along the z axis is shown in Fig. 1. The nuclear motion is restricted to the polarization direction of the laser electric field, while the muon μ moves in three dimensions with conservation of cylindrical symmetry. Accordingly, two coordinates of the muon, z and ρ, measured with respect to the center of mass of proton p and deuteron d, are treated explicitly together with the internuclear separation R.

The heteronuclear $pd\mu$ system has a permanent dipole moment. The component of the dipole operator along the z axis is a function of R and z and reads [10]

$$\hat{d}_z(R,z) = -e\{R(M_\mathrm{d} - M_\mathrm{p})/(M_\mathrm{d} + M_\mathrm{p}) + z[1 + M_\mu/(M_\mathrm{d} + M_\mathrm{p} + M_\mu)]\}, \quad (1)$$

where e is the muon charge and M_d, M_p, and M_μ are the deuteron, proton, and muon masses, respectively. M_μ is 206.768 times the electron mass M_e, the latter defining the atomic mass unit. Due to the permanent dipole moment, vibrational motion in $pd\mu$ is excited both directly, by the laser field, and also indirectly, due to the muon motion. At the same time, the laser-driven muonic motion along the optically active z degree of freedom induces muonic motion along the optically passive transversal ρ degree of freedom due to the wave properties of the muon.

In contrast, the homonuclear $pp\mu$ system does not have a permanent dipole moment. The component of the dipole operator of $pp\mu$ along the z axis is a function of z only and reads

$$\hat{d}_z(z) = -ez[1 + M_\mu/(2M_\mathrm{p} + M_\mu)]. \quad (2)$$

Therefore, vibrational motion in $pp\mu$ is excited only indirectly—due to the muonic motion induced by the laser field along the z axis [11–13]. Muonic motion along the optically passive transversal ρ degree of freedom occurs only due to the wave properties of the muon.

The time-dependent Schrödinger equation describing the quantum dynamics of $pd\mu$ in the classical laser field (Fig. 1) reads

$$i\hbar\frac{\partial}{\partial t}\Psi = -\frac{\hbar^2}{2m_\mathrm{n}}\frac{\partial^2\Psi}{\partial R^2} - \frac{\hbar^2}{2m_\mu}\left(\frac{\partial^2\Psi}{\partial\rho^2} + \frac{1}{\rho}\frac{\partial\Psi}{\partial\rho}\right) - \frac{\hbar^2}{2m_\mu}\frac{\partial^2\Psi}{\partial z^2} + V_C(R)\Psi - V_C(r_1)\Psi - V_C(r_2)\Psi - d_z(R,z)\mathcal{E}(t)\Psi. \quad (3)$$

In Eq. (3), $\Psi(R,z,\rho,t)$ is the total wave function, $m_\mathrm{n} = M_\mathrm{d}M_\mathrm{p}/(M_\mathrm{d} + M_\mathrm{p})$ is the nuclear reduced mass, and $m_\mu = M_\mu(M_\mathrm{d} + M_\mathrm{p})/(M_\mu + M_\mathrm{d} + M_\mathrm{p})$ is the muon reduced mass. The Coulomb potentials V_C are treated, similar to Ref. [1], within the nuclear drop model as follows.

For the proton-deuteron interaction, the Coulomb potential

$$V_C(R) = \frac{e^2}{r_\mathrm{p} + r_\mathrm{d}}\left[\frac{3}{2} - \frac{R^2}{2(r_\mathrm{p} + r_\mathrm{d})^2}\right] \quad \text{if } R \leqslant r_\mathrm{p} + r_\mathrm{d} \quad (4)$$

and $V_C(R) = 1/R$ if $R > r_\mathrm{p} + r_\mathrm{d}$, where $r_\mathrm{p} = 0.8751$ fm and $r_\mathrm{d} = 2.1413$ fm are the proton and deuteron charge radii, respectively (1 fm $= 10^{-15}$ m). The Coulomb potential $V_C(r)$ for the muon-nucleus interaction reads

$$V_C(r) = \frac{e^2}{r_\mathrm{n}}\left[\frac{3}{2} - \frac{r^2}{2r_\mathrm{n}^2}\right] \quad \text{if } R \leqslant r_\mathrm{n} \quad (5)$$

and $V_C(r) = 1/r$ if $r > r_\mathrm{n}$, where the nuclear radius r_n stands for r_p or r_d, specified above, and r stands for the muon-proton r_1 or muon-deuteron r_2 distances, which read

$$r_1(R,\rho,z) = \{\rho^2 + [z + RM_\mathrm{d}/(M_\mathrm{d} + M_\mathrm{p})]^2\}^{1/2} \quad (6)$$

and

$$r_2(R,\rho,z) = \{\rho^2 + [z - RM_\mathrm{p}/(M_\mathrm{d} + M_\mathrm{p})]^2\}^{1/2}, \quad (7)$$

respectively (see Fig. 1). In the case of homonuclear $pp\mu$, the deuteron mass M_d should be replaced with the proton mass M_p with straightforward modifications of Eqs. (3)–(7).

The laser field $\mathcal{E}(t)$ in Eq. (3) is chosen as a single five-cycle pulse with a smooth shape,

$$\mathcal{E}(t) = \mathcal{E}_0\, S(t)\sin(\omega_l t), \quad (8)$$

where the shape $S(t)$ comprises one cycle for the smooth $\sin^2$-type turn-on, followed by three cycles with the amplitude $\mathcal{E}_0$ and one cycle for the smooth $\sin^2$-type turn-off of the pulse. The laser-pulse amplitude is $\mathcal{E}_0 = 1 \times 10^3$ a.u. (atomic electric field unit, 1 a.u. $= 5.14 \times 10^{14}$ V/m), which corresponds to a peak intensity $I_0 = \frac{1}{2}c\varepsilon_0\mathcal{E}_0^2 = 3.51 \times 10^{22}$ W/cm^2. The laser carrier frequency times $\hbar$ is $\hbar\omega_l = 2.1682$ a.u., where a.u. is the atomic energy unit [1 a.u. $= 1E_h$(Hartree) $= 27.2114$ eV], i.e., $\hbar\omega_l = 59$ eV. The overall pulse duration is $t_p = 0.35$ fs (1 fs $= 10^{-15}$ s). The pulse parameters are the same as those used in Ref. [1], except for the intensity which was higher there. The pulse is shown in Fig. 2(c) below. We also notice that with the laser carrier frequency $\hbar\omega_l = 2.1682$ a.u. used in the present work, the laser wavelength, $\lambda_l = 396.912$ a.u.,

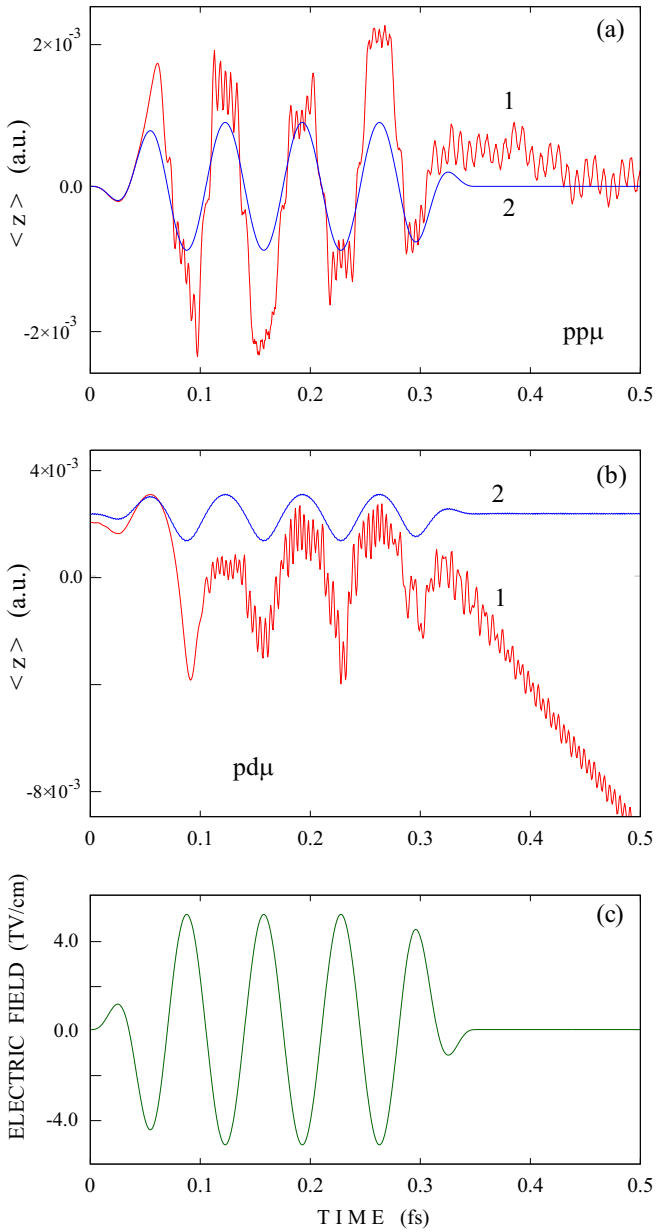

FIG. 2. Laser-driven quantum dynamics and the initial stage of post-laser-pulse free evolution of $pp\mu$ (a) and $pd\mu$ (b). Time-dependent expectation values $\langle z\rangle$ of the laser-driven muonic degree of freedom z: curves 1—the non-Born-Oppenheimer treatment; curves 2—the Born-Oppenheimer approximation. (c) The five-cycle shaped laser pulse: $\mathcal{E}_0 = 1 \times 10^3$ a.u. ($I = 3.51 \times 10^{22}$ W/cm^2), $\omega_l = 2.1682$ a.u. ($\hbar\omega_l = 59$ eV), and $t_p = 0.35$ fs.

is by more than three orders of magnitude larger than the size of diatomic muonic ions, which was estimated from above in Ref. [13] as 0.1 a.u. Hence the electric dipole approximation used in the equation of motion (3) is well justified.

Numerical techniques used to solve the 3D equation of motion (3) have been described in detail in previous works [13,14]. Specific details are given in Appendix A. Besides undergoing bound motion, the molecules may also dissociate or ionize. The dissociation probability was calculated with the time- and space-integrated outgoing flux for the nuclear coordinate R; the ionization probabilities were calculated with the respective fluxes separately for the positive and the negative direction of the z axis as well as for the outer end of the ρ axis. The other decay process occurring in muonic molecules, nuclear fusion at a very small internuclear separation, can be neglected in $pp\mu$ and $pd\mu$ due to a very small fusion rate [9]. Therefore, nuclear fusion was not taken into account in our present work.

Initially, at $t = 0$, $pp\mu$ and $pd\mu$ were assumed to be in their ground vibrational states. The wave functions of the initial states were obtained by the numerical propagation of the equation of motion (3) in imaginary time without the laser field ($\mathcal{E}_0 = 0$). The energy of the ground states was $E = -102.2251$ a.u. (E_h) for $pp\mu$ and $E = -106.0146$ a.u. for $pd\mu$. Considering the ground-state energy of muonic H and D, of $E_{p\mu} = -0.5(M_\mu \cdot M_\mathrm{p})/(M_\mu + M_\mathrm{p})$ a.u. $= -92.9202$ a.u. and $E_{d\mu} = -0.5(M_\mu \cdot M_\mathrm{d})/(M_\mu + M_\mathrm{d})$ a.u. $= -97.8707$ a.u., respectively, we have binding energies E_bind of these ground states with respect to the dissociation limit, of $E_\mathrm{bind} = 102.2251 - 92.9202 = 9.3050$ a.u. (or 253.2 eV) and 8.1439 a.u. (or 221.6 eV) for $pp\mu$ and $pd\mu$, respectively. Further, the maximal R-probability density of these states was at $R = 0.011$ a.u. ($pp\mu$) and at $R = 0.015$ a.u. ($pd\mu$), respectively (1 a.u. = 1 Bohr unit $a_0 = 0.5292 \times 10^{-10}$ m).

To put these numbers and also the laser parameters in a broader context, we note that a Born-Oppenheimer potential-energy surface of a muonic hydrogenic molecular ion can be estimated from simply using the analogy to the corresponding electronic molecular ion, H_2^+, and replacing there the Bohr unit a_0 by the corresponding muonic Bohr unit $a_\mu = a_0 M_e/M_\mu = 0.0048 a_0$ [9]. Similarly, the electronic atomic energy unit E_h should be replaced by $E_\mu = E_h M_\mu/M_e = 206.768 E_h$. The H_2^+ has a ground-state potential-energy surface with a classical minimum at $R_0 \simeq 2a_0$, about $0.1E_h$ (2.7 eV) deeper than the dissociation limit (H+H$^+$), with an energy of $-0.5E_h$. A corresponding muonic species, $pp\mu$, has therefore $R_0 \simeq 0.0097 a_0 \simeq 5.1 \times 10^{-13}$ m, and a (classical) dissociation energy of $\sim 20.7 E_h \sim 563$ eV. According to Ref. [9], both $pp\mu$ and $pd\mu$ have only a single bound vibrational state, with (nonclassical) dissociation energies of 253.15 eV ($pp\mu$) and 221.55 eV ($pd\mu$), respectively. These values are in very good agreement with our computed binding energies and, considering the potential-energy picture, show that the zero-point energy is about half of the classical dissociation energy. Further, from our calculations above we note that the maxima of the R distributions of the ground states are located at slightly higher R than the classical value R_0 as expected. Finally, the laser energy of 59 eV is clearly below the dissociation and ionization energies of the molecular ions, so that these events can only occur *via* multiphoton processes.

III. LASER-DRIVEN DYNAMICS AND FREE EVOLUTION OF $pp\mu$ AND $pd\mu$ AFTER THE END OF THE LASER PULSE

Excitation of $pp\mu$ and $pd\mu$ by the 0.35 fs laser pulse and the initial stage of their free evolution after the end of the pulse (up to 0.5 fs) are presented in Fig. 2 by the time-dependent expectation values $\langle z\rangle$ of the optically active muonic degree of freedom z. The non-Born-Oppenheimer quantum dynamics of

$pp\mu$ and $pd\mu$ are shown in Figs. 2(a) and 2(b), respectively, by curves 1. For the sake of comparison, results obtained at fixed internuclear distances, $R = 0.0125$ a.u. for $pp\mu$ and $R = 0.015$ a.u. for $pd\mu$, which are close to the respective classical equilibrium value R_0 (and the maximum of R distributions; see above), are presented in Figs. 2(a) and 2(b) by curves 2. Results obtained at fixed internuclear distances are referred to as those obtained within the Born-Oppenheimer approximation. Finally, the driving shaped five-cycle laser pulse is shown in the bottom, Fig. 2(c).

From Fig. 2 it is clear that there are pronounced differences between the non-Born-Oppenheimer and the Born-Oppenheimer treatments. We see that the muon treated beyond the Born-Oppenheimer approximation follows the applied laser field out of phase (expectation values $\langle z\rangle$ increase when the field strength decreases) only approximately. At the end of the pulse the muonic motion along the z coordinate is still excited, which results in post-laser-pulse muonic z oscillations occurring in both $pp\mu$ and $pd\mu$ [see curves 1 in Figs. 2(a) and 2(b)]. In case of $pd\mu$, $\langle z\rangle$ values become more and more negative in average after the pulse is off, indicating the onset of a large-amplitude motion of the muon. In contrast, within the Born-Oppenheimer approximation a perfect muon-field out-of-phase following takes place during the laser pulse. At the end of the pulse, expectation values $\langle z\rangle$ return back to their initial equilibrium ones and the post-laser-pulse muonic oscillations do occur neither in $pp\mu$ nor in $pd\mu$ [see curves 2 in Figs. 2(a) and 2(b)]. Similar differences were obtained in previous work [8] for $dd\mu$ and $dt\mu$, albeit less striking. However, also there oscillations were present after the pulse only in the non-Born-Oppenheimer case, such that the existence of post-laser-pulse muonic oscillations in small muonic molecular ions can be considered entirely a non-Born-Oppenheimer phenomenon.

IV. DISSOCIATION, IONIZATION, AND POSTLASER MUONIC AND NUCLEAR OSCILLATIONS ON A LONGER TIME SCALE

Since very intense laser pulses were used for the initial excitation of $pp\mu$ and $pd\mu$, it is important to estimate first a possible role of ionization and dissociation with respect to the post-laser-pulse free evolution on a long time scale. Time-dependent ionization and dissociation probabilities of $pp\mu$ and $pd\mu$ are plotted in Fig. 3 on a longer time scale of 43 fs. Dissociation probabilities are presented by curves $D(t)$ and ionization probabilities for the positive or negative directions of the z axis are presented by curves $I_{z(\pm)}$, respectively. Ionization probabilities for the outer end of the ρ axis at $t = 43$ fs are comparatively very small, $I_\rho = 0.57 \times 10^{-5}$ for $pp\mu$ and 0.11×10^{-4} for $pd\mu$, and are not plotted in Fig. 3.

It is seen from Fig. 3 that both ionization and dissociation of $pd\mu$ is significantly higher as compared to $pp\mu$. Nevertheless, the respective probabilities are rather small: the overall dissociation and ionization yield (including that for the ρ degree of freedom) is about 0.38% for $pd\mu$ and only about 0.12% for $pp\mu$. Hence post-laser-pulse muonic and nuclear oscillations of $pp\mu$ and $pd\mu$ are practically not affected by ionization and dissociation.

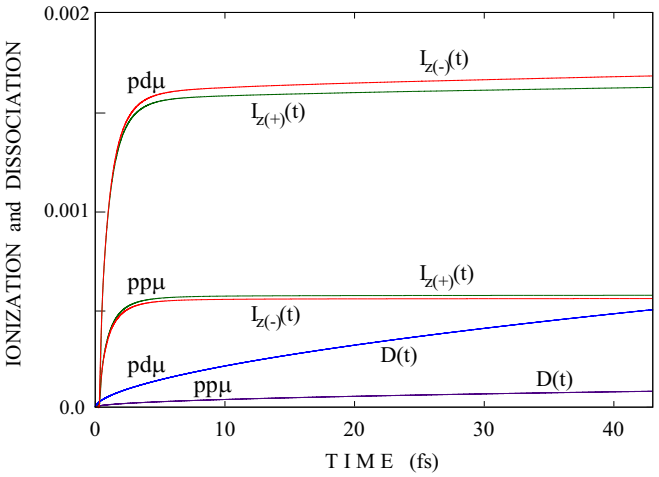

FIG. 3. Time-dependent ionization and dissociation probabilities of $pp\mu$ and $pd\mu$. Curves $I_{z(+)}(t)$ and $I_{z(-)}(t)$ present ionization probabilities in the positive and in the negative direction of the z axis, respectively. Curves $D(t)$ present the dissociation probabilities.

Returning to the laser-induced muonic z oscillations already reported in Fig. 2, we now discuss their evolution on the longer time scale up to $\simeq$43 fs. This is done for $pp\mu$ and $pd\mu$ in Fig. 4(a). The time-dependent expectation values $\langle z\rangle$ shown there demonstrate quite complicated fast oscillations with various modulations which are more clearly seen in a shorter time interval [29,30] fs in Fig. 4(b).

We also may identify characteristic frequencies of z oscillations which often play the role of a "carrier" frequency of post-laser-pulse oscillations in muonic [8] and electronic [15,16] molecular ions. In order to do so, we consider even shorter time intervals. In Figs. 4(c) and 4(d), the time-dependent expectation values $\langle z\rangle$ of $pp\mu$ and $pd\mu$ are presented on a very narrow time interval of 0.3 fs in the range [30.4,30.7] fs. It is possible to reveal from there that the period of muonic z oscillations is $\tau_z^{\rm osc} \simeq 8.25 \times 10^{-3}$ fs in $pp\mu$ and $\tau_z^{\rm osc} \simeq 4.69 \times 10^{-3}$ fs in $pd\mu$, implying the characteristic frequencies of $\omega_z^{\rm osc} \simeq 18.421$ a.u. for $pp\mu$ and $\omega_z^{\rm osc} \simeq 32.406$ a.u. for $pd\mu$. The ratios of characteristic frequencies of muonic z oscillations to the laser carrier frequency $\omega_l = 2.1682$ a.u. are about 8.496 for $pp\mu$ and 14.946 for $pd\mu$ in the chosen interval. One can conclude, therefore, that both $pp\mu$ and $pd\mu$ may generate frequencies of z oscillations which are not equal to pure integer multiples of the laser carrier frequency. By Fourier analyzing the $\langle z(t)\rangle$ curves of Fig. 4(a), we find also other frequencies, not necessarily integer multiples of ω_l (not shown). It can be imagined that characteristic oscillations translate into signals in power (or HHG) spectra. The fact that single atoms and molecules may emit harmonics that are different from pure integer multiples of the laser carrier frequency can be explained by resonance effects, as it was already discussed earlier [17,18]. It will be interesting to see, therefore, if such resonance effects will manifest themselves in power and HHG spectra related to the z degree of freedom of $pp\mu$ and $pd\mu$ to be discussed in the next section.

Before doing so, we now consider degrees of freedom other than z. In contrast to the laser driven z degree of freedom, the transversal ρ degree of freedom of $pp\mu$ and $pd\mu$ is

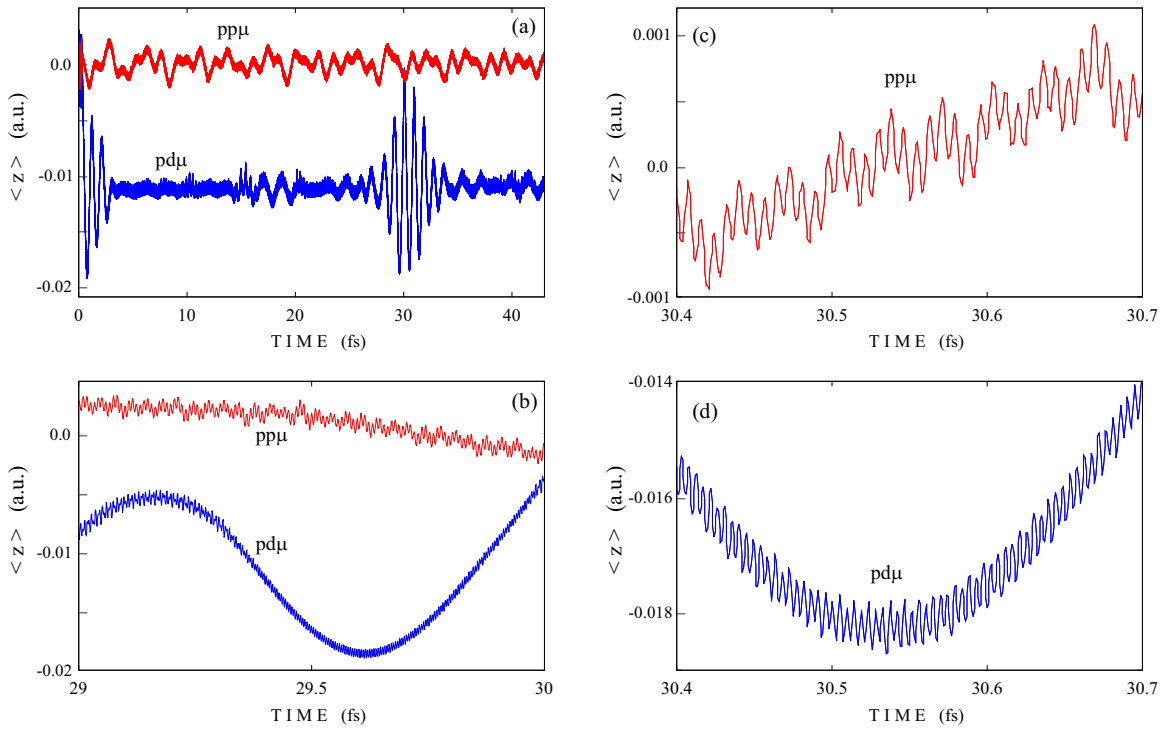

FIG. 4. Time-dependent expectation values $\langle z\rangle$ of $pp\mu$ and $pd\mu$ on a time scale from 0 to $\simeq$43 fs (a) and in a short-time interval [29, 30] fs (b). The same on a very short-time interval [30.4, 30.7] fs for $pp\mu$ (c) and $pd\mu$ (d).

optically passive and excited only due to the wave properties of the muon. Time-dependent expectation values $\langle\rho\rangle$ of $pp\mu$ and $pd\mu$ are shown in Fig. 5(a) on the time scale including their excitation by the 0.35 fs laser pulse followed by the stage of free evolution, up to 1.6 fs. It is seen that both $pp\mu$ and $pd\mu$ demonstrate after the end of the pulse coherent ρ oscillations—temporarily shaped in the case of $pd\mu$ and with nearly permanent amplitude in the case of $pp\mu$. Such a behavior can be explained by the Coulombic interaction of the muon and nuclei.

Time-dependent expectation values $\langle R\rangle$ of the internuclear distance of $pp\mu$ and $pd\mu$ are presented in Fig. 5(b). Since $pd\mu$ has a permanent dipole moment, its internuclear distance changes much more substantially as compared to $pp\mu$. Indeed, it is clearly seen from Fig. 5(b) that the internuclear distance in $pd\mu$ has a well pronounced minimum at $t \approx 1.2$ fs, which is well correlated with the maximum of ρ oscillations in Fig. 5(a). The physical reason is that when nuclei in $pd\mu$ come close to each other, the component of the Coulomb force on the transversal ρ degree of freedom increases and the amplitude of ρ oscillations in $pd\mu$ rises accordingly. In contrast, since the internuclear distance in $pp\mu$ does not change substantially [Fig. 5(b)], the amplitude of ρ oscillations in $pp\mu$ remains nearly unchanged [Fig. 5(a)].

It can be found from the results presented in Fig. 5(a) on the time interval $0.6\,\text{fs} \leqslant t \leqslant 0.9$ fs that the period of muonic ρ oscillations is $\tau_\rho^{\text{osc}} \simeq 1.087 \times 10^{-2}$ fs in $pp\mu$ and $\tau_\rho^{\text{osc}} \simeq 4.65 \times 10^{-3}$ fs in $pd\mu$, implying the characteristic frequencies of $\omega_\rho^{\text{osc}} \simeq 13.981$ a.u. for $pp\mu$ and $\omega_\rho^{\text{osc}} \simeq 32.684$ a.u. for $pd\mu$. The ratios of characteristic frequencies of muonic ρ oscillations to the laser carrier frequency $\omega_l = 2.1682$ a.u. are about 6.448 for $pp\mu$ and 15.074 for $pd\mu$. Again, for this time regime at least we can conclude that both $pp\mu$ and $pd\mu$ may generate frequencies of ρ oscillations that are not equal to integer multiples of the laser carrier frequency [18].

Needless to add that nuclear motion strongly influences the post-laser-pulse oscillations of the optically active z degree of freedom as well, which is especially prominent on a long time scale in the case of $pd\mu$ [see Fig. 5(c)]. It goes without saying that muonic motion along the z axis influences nuclear motion in its turn, and the non-Born-Oppenheimer quantum dynamics and free evolution of any degree of freedom represents the combined effect of all degrees of freedom. In Fig. 5(c), time-dependent expectation values $\langle R\rangle$ and $\langle z\rangle$ of $pd\mu$ are plotted on the long time scale of ca. 43 fs. Both curves presented in Fig. 5(c) have a very complicated fine structure as a consequence of the fact that both expectation values, $\langle R\rangle$ and $\langle z\rangle$, demonstrate rather complicated fast oscillations with various modulations similar to those presented in Fig. 4 and discussed above. The characteristic feature of the "coarse-grained" expectation values $\langle R\rangle$ and $\langle z\rangle$ presented in Fig. 5(c) is that they evolve out of phase with each other, as indicated by vertical arrows therein. Indeed, local minima of the bond length $\langle R\rangle$ correspond to the local maxima of $\langle z\rangle$ and vice versa. Such muon-nuclei correlations can be explained, similar to the temporal shaping of muonic ρ oscillations in $pd\mu$ [Fig. 5(a)] due to contraction and elongation of the bond length of $pd\mu$ [Fig. 5(b)], by the muon-nuclei Coulombic interactions. Similar electron-nuclei correlations in the electronic molecular ion H_2^+ were explained in detail in previous works [15,16] both in terms of time-dependent expectation values $\langle R\rangle$ and $\langle z\rangle$ and in terms of the time-dependent electron acceleration $\langle -\partial V/\partial z\rangle$.

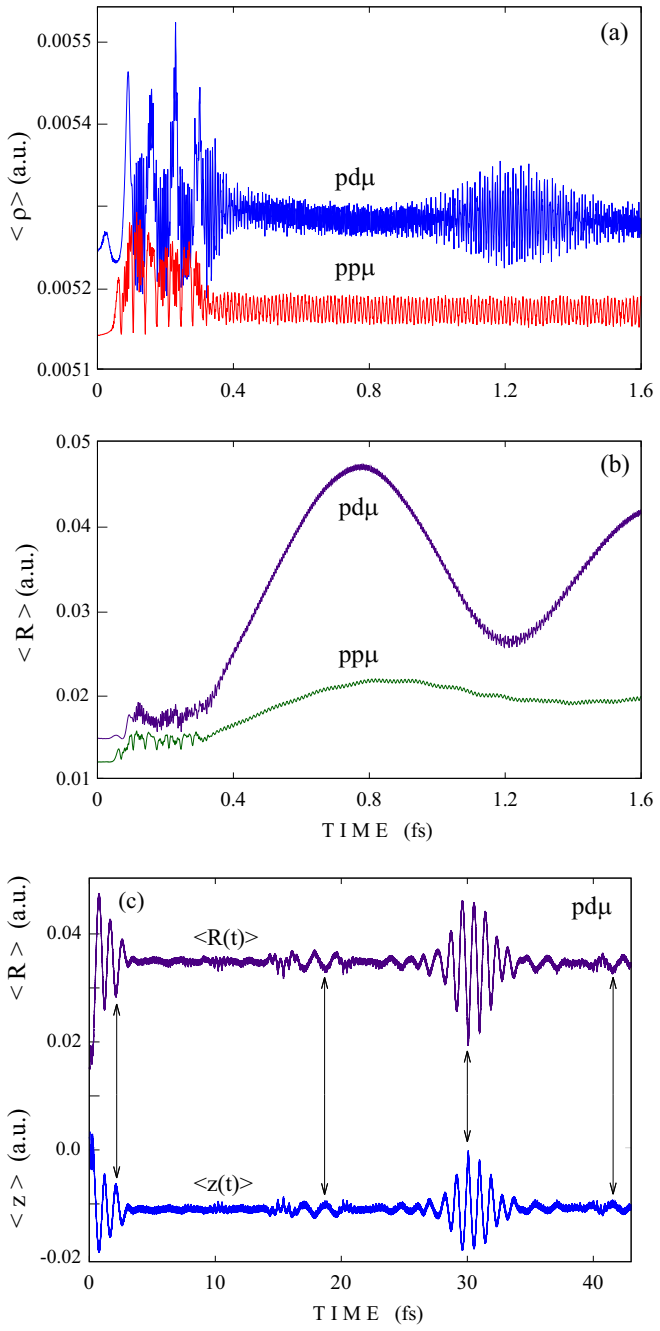

FIG. 5. (a) Time-dependent expectation values $\langle\rho\rangle$ of $pp\mu$ and $pd\mu$ on a short-time scale [0,1.6] fs revealing the period of muonic ρ oscillations. (b) Corresponding time-dependent internuclear distances $\langle R\rangle$. (c) Time-dependent expectation values $\langle R\rangle$ and $\langle z\rangle$ of $pd\mu$ on a long time scale in a "coarse-grained" representation. Vertical arrows illustrate the fact that $\langle R(t)\rangle$ and $\langle z(t)\rangle$ evolve *out of phase* with each other.

It is clearly seen from Fig. 5(c) that sequential contractions and elongations of the bond length and substantial muonic excursions in the positive-negative direction of the z axis are especially prominent at around $t \approx 30$ fs where they appear as "full-length" shaped pulses presenting the "echo pulses" of "half-length" pulses that appeared earlier on the time interval $0 \leqslant t \leqslant 4$ fs. Note that such echo pulses do not appear in the

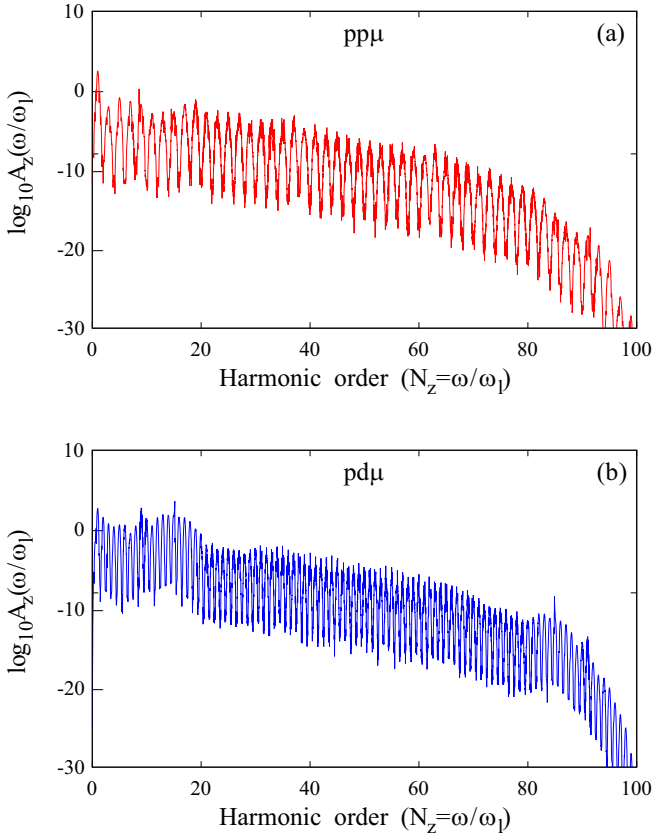

FIG. 6. Power spectra $A_z(\omega)$ of $pp\mu$ (a) and $pd\mu$ (b) in a wide frequency domain, up to $\omega/\omega_l = 100$.

homonuclear $pp\mu$ ion excited by the same laser pulse as $pd\mu$ under discussion. On the other hand, it was shown in previous work [8] that similar shaped echo pulses appeared in the homonuclear $dd\mu$ ion but did not appear in the heteronuclear $dt\mu$ ion when both were excited by identical superintense attosecond x-ray laser pulses at $\lambda_l = 5$ nm. We can conclude, therefore, that the appearance of echo pulses, similar to those presented in Fig. 5(c), strongly depends on the type of the laser pulse used to excite a system under study.

V. POWER AND HHG SPECTRA GENERATED BY $pp\mu$ AND $pd\mu$

In this section we present the power spectra generated by muonic degrees of freedom z, ρ and by the nuclear degree of freedom R of $pp\mu$ and $pd\mu$ calculated in the acceleration form, i.e.,

$$A_k(\omega) = \propto \left| \int_0^{t_f} e^{-i\omega t} \frac{d^2}{dt^2} \langle \Psi(t)|k|\Psi(t)\rangle \, dt \right|^2, \qquad (9)$$

where $k = z$, ρ, or R, and $t_f \simeq 43$ fs is the total propagation time. The integrand in Eq. (9) was resolved with a time step of $\Delta t = 7.0097 \times 10^{-4}$ fs. The maximal frequency in $A_k(\omega)$ we can represent is then $\omega_{\max} = 2\pi/\Delta t$, or $\hbar\omega_{\max} \simeq 217$ a.u. We can, therefore, resolve up to $N_{\max} = \omega_{\max}/\omega_l \simeq 100$ harmonics. All power spectra are presented below as functions of frequency ω in units of the laser carrier frequency $\omega_l = 2.1682$ a.u. ($\hbar\omega_l = 59$ eV), with the proportionality constant

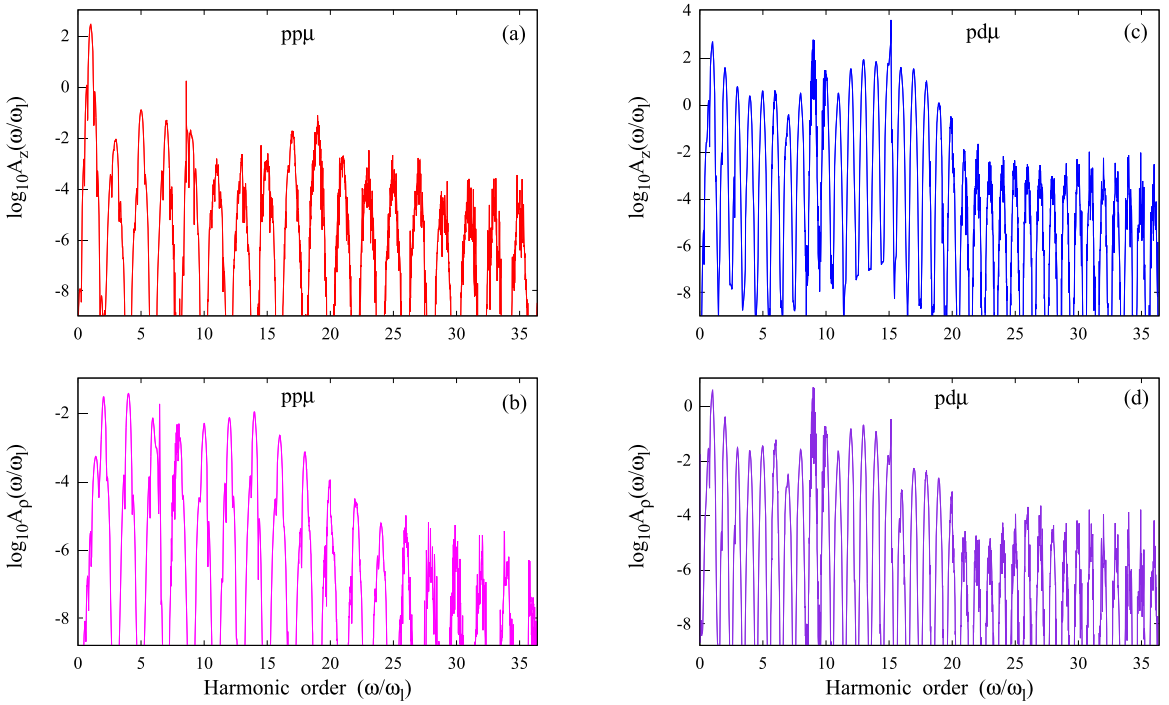

FIG. 7. Power spectra $A_z(\omega)$ and $A_\rho(\omega)$ of $pp\mu$ (left panel) and $pd\mu$ (right panel) in a narrow frequency domain.

in (9) set to 1 and the amplitude given in atomic units. Some HHG spectra are presented in both acceleration and length form (see Fig. 10 below). Although the acceleration form is more time consuming, since accelerations are calculated at every time step of propagations, it is preferable for power spectra because any acceleration is directly related to the force acting along the corresponding degree of freedom.

Note that the power spectra $A_k(\omega)$ are closely related to HHG spectra. For instance, for $pp\mu$, the z component of the dipole operator is given by Eq. (2) as $\hat{d}_z = az$ (where $a = -e1.0533$), $\frac{d^2}{dt^2}\langle\Psi(t)|z|\Psi(t)\rangle \propto \frac{d^2}{dt^2}\langle\Psi(t)|\hat{d}_z|\Psi(t)\rangle$, and, therefore, the signal $A_z(\omega)$ is directly proportional to the z component of the HHG spectrum of that molecule. For $pd\mu$, the situation is slightly more complicated as shown below, with both $A_z(\omega)$ and $A_R(\omega)$ contributing to a z-polarized HHG signal of the molecule.

In Fig. 6, power spectra $A_z(\omega)$, generated due to the laser-induced muonic motion along the z coordinate of $pp\mu$ and $pd\mu$, are presented in a wide frequency domain, up to $\omega/\omega_l = 100$.

For $pd\mu$ (b) we first of all note a a rapid decay of the HHG signal up to $\omega/\omega_l \simeq 20$, followed by a more slowly decaying plateau region and a further decay around $\omega/\omega_l \simeq 90$. For $pp\mu$ similar behavior is found, with slightly less structured transitions. We should note that according to classical estimates of the cutoff in HHG spectra, based on the three-step model and a continuous-wave driving field [19], one has

$$\hbar\omega_{\rm cut} = {\rm IP} + 3.17U_p, \tag{10}$$

where IP is the ionization potential of the system and U_p the ponderomotive energy. The latter is defined, for an electronic system, in atomic units as $U_p = \mathcal{E}_0^2/(4M_e\omega_l^2)$. As shown in Appendix B, a very simple estimate of $\hbar\omega_{\rm cut}$ based on a vertical ionization potential and a ponderomotive energy where M_e is simply replaced by M_μ gives (i) a cutoff $N_{\rm cut} = \omega_{\rm cut}/\omega_l$ around 470, (ii) with (ii) small differences between $pp\mu$ and $pd\mu$. Therefore, the "true" cutoff regions of HHG spectra of $pp\mu$ and $pd\mu$ are not yet reached in Fig. 6 and some differences are to be expected for the overall shape of HHG spectra of both isotopomers. The latter is in agreement with our findings. Differences in (the cutoff region of) HHG spectra of atomic $p\mu$ and $d\mu$ have also been observed in Refs. [1,3].

The main, striking difference between the power spectra generated by the optically active z degree of freedom of $pp\mu$ [Fig. 6(a)] and $pd\mu$ [Fig. 6(b)], however, is the appearance in the latter case of even harmonics due to inversion symmetry breaking in the heteronuclear $pd\mu$ system, similar to $dt\mu$ [8] and the electronic HD molecule [18].

In Figs. 7(a) and 7(c), we analyze the HHG spectra of $pp\mu$ and $pd\mu$ for the muonic z mode in some more detail, focusing on harmonics up to $\simeq$36. Further, we analyze HHG spectra of $pp\mu$ and $pd\mu$ for the muonic ρ coordinate in Figs. 7(b) and 7(d). It is now also more clearly seen from Fig. 7(a) that only odd harmonics of muonic z oscillations (harmonic order $N_z = 2n-1$, $n = 1,2,3,\ldots$) are generated in $pp\mu$, while for $pd\mu$ also even harmonics occur [Fig. 7(c)].

The transversal ρ degree of freedom of the muon in $pp\mu$ and $pd\mu$ is optically passive if the laser field is aligned along the z axis and muonic ρ oscillations can be excited only due to the wave properties of the muon and muonic z oscillations. Nevertheless, ρ oscillations are clearly seen as shown in Figs. 7(b) and 7(d). Considering $pp\mu$ in Fig. 7(b), in contrast to the case of z oscillation leading to only odd harmonics, now only *even* harmonics (harmonic order $N_\rho = 2n$) are generated due to muonic ρ oscillations. Such a "frequency doubling" of laser induced muonic z oscillations by optically passive muonic ρ oscillations can be explained on the basis of previous

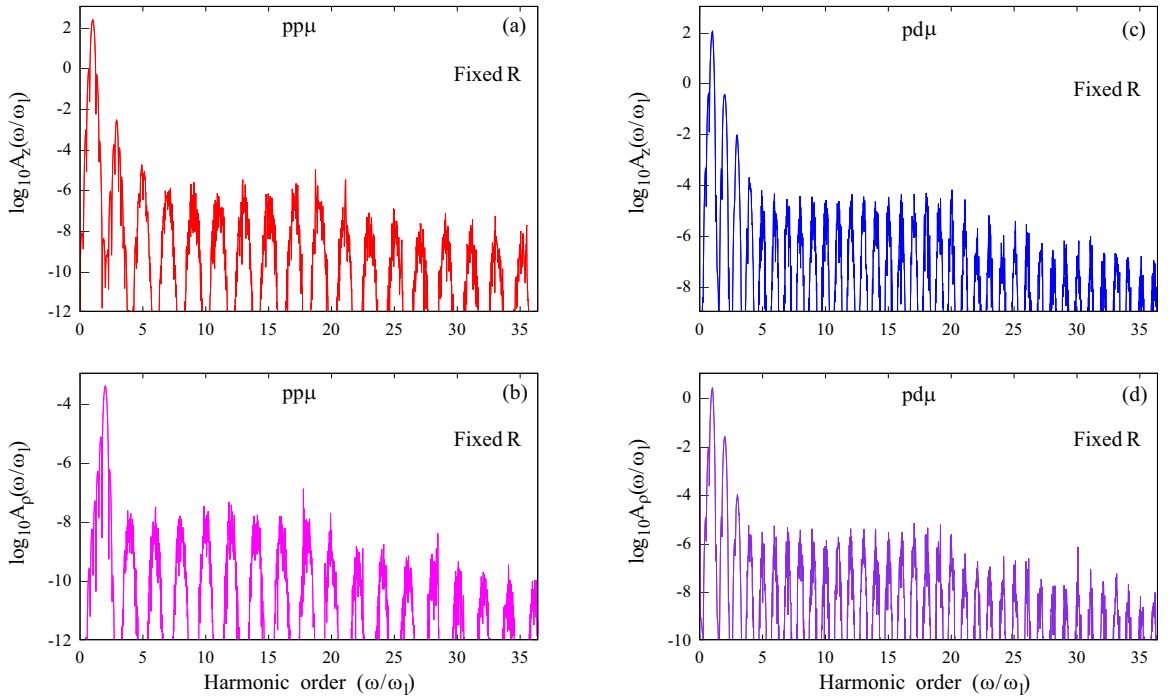

FIG. 8. Power spectra $A_z(\omega)$ and $A_\rho(\omega)$ of $pp\mu$ (left panel) and $pd\mu$ (right panel) in a narrow frequency domain, now in the Born-Oppenheimer approximation ("fixed R").

works [13,14] as follows. During the laser-induced muonic z oscillations, the muonic density is delocalized also in the transversal ρ direction due to the wave properties of the muon. This happens twice per each cycle of muonic z oscillations at every turning point of the muon, thus giving rise to muonic ρ oscillations at $\omega_\rho^{\rm osc} \approx 2\omega_z^{\rm osc}$. Indeed, at a close look at Fig. 5(a), it can be concluded from the time intervals between the first lowest minima of the ρ curve of $pp\mu$ that the second harmonic, $\omega_\rho \approx 2\omega_l$, appears already during the 0.35 fs laser pulse. It is easy to see that the effect of frequency doubling gives rise initially to ρ harmonics with harmonic number $N_\rho^{(i)} = 4n - 2$, while the other positions in the $A_\rho(\omega)$ spectrum of Fig. 7(b) can be filled in due to combined effects of any two initial $N_\rho^{(i)}$ harmonics. Note that similar results were obtained for the homonuclear $dd\mu$ ion in previous work [8].

From Fig. 7(d), where the $A_\rho(\omega)$ spectrum for $pd\mu$ is shown it is seen that, in contrast to $pp\mu$, both odd and even harmonics are generated due to the muonic motion along the ρ coordinate. While the existence of even harmonics in the $A_z(\omega)$ spectrum [Fig. 7(c)] can be explained by inversion symmetry breaking in the heteronuclear $pd\mu$ ion [18], as it was just discussed above, the appearance of both even and odd harmonics in the $A_\rho(\omega)$ spectrum of $pd\mu$ requires a more detailed explanation. On the one hand, it is easy to see that, similar to $pp\mu$, only even harmonics $N_\rho^{(i)} = 2n$ are generated in the $A_\rho(\omega)$ spectrum of $pd\mu$ due to the effect of frequency doubling of muonic z oscillations. On the other hand, at a close look at Fig. 5(a), it can be concluded from the time intervals between the four first highest maxima of the ρ curve of $pd\mu$ that the first harmonic, $\omega_\rho \approx \omega_l$, appears already during the 0.35 fs laser pulse. Therefore, the appearance of the odd harmonics in the $A_\rho(\omega)$ spectrum of $pd\mu$ [Fig. 7(d)] can be explained by combined effects of the first harmonic $N_\rho = 1$ that appeared during the laser pulse and even harmonics $N_\rho^{(i)} = 2n$ that appeared due to the effect of frequency doubling. Similar results—the existence of both odd and even harmonics in power spectra generated due the 2D muonic motion in the heteronuclear $dt\mu$ ion—were obtained in previous work [8].

It is also seen from Fig. 7 that some harmonics of the power spectra generated by the muonic motion in $pp\mu$ and $pd\mu$ have quite a complicated structure, including, e.g., very sharp maxima at around $N_z = 9$ and $N_\rho = 6$ in $pp\mu$ [Figs. 7(a) and 7(b)], as well as at around the 15th harmonics in both $A_z(\omega)$ and $A_\rho(\omega)$ spectra of $pd\mu$ [Figs. 7(c) and 7(d)]. Such spectral features can be explained by resonance effects in isolated atoms and molecules [17,18]. In particular, all three aforementioned sharp maxima in power spectra, whose exact positions are $\omega/\omega_l = 8.5879$, 6.4676, and 15.149, respectively, are related quite well to characteristic frequencies of muonic z and ρ oscillations estimated in the previous section as follows: $\omega_z^{\rm osc}/\omega_l \simeq 8.496$ and $\omega_\rho^{\rm osc}/\omega_l \simeq 6.448$ for $pp\mu$; $\omega_z^{\rm osc}/\omega_l \simeq 14.946$ and $\omega_\rho^{\rm osc}/\omega_l \simeq 15.074$ for $pd\mu$. We can conclude, therefore, that characteristic frequencies of muonic post-laser-pulse oscillations manifest themselves by very sharp maxima in the corresponding power spectra.

Again, it is interesting to quantify the effect of nuclear motion on power and HHG spectra. In Fig. 8 the analogous information to Fig. 7 is given, however, with the internuclear distance R fixed: to $R = 0.0125$ a.u. for $pp\mu$ and to $R = 0.015$ a.u. for $pd\mu$, respectively, as above.

When comparing the two figures, Figs. 7 and 8, we note that the overall shape and the general "selection rules" (i.e., the occurrence of odd or even or both harmonics) do not change under the Born-Oppenheimer approximation. This is already interesting because in Ref. [18] for a model of (also asymmetric) HD (in which electrons and nuclei were allowed

to move along the molecular axis only), it had been found that even harmonics were only seen beyond the Born-Oppenheimer approximation.

However, we find also differences between the power spectra of $pp\mu$ and $pd\mu$ molecular ions in important details. The most striking difference is that the intensity ratio between the lowest visible harmonic (the first or the second) and the following, higher-order harmonics increases substantially in the Born-Oppenheimer case. In fact, the intensity of almost all harmonics higher than the first ones, lose substantially in intensity when the nuclei don't move, for all cases studied. A simple explanation of the lower intensity in the Born-Oppenheimer case can already be drawn from Figs. 2(a) and 2(b): there it is clearly seen that, for instance, the amplitudes of $\langle z\rangle$ are smaller and the whole curves are much smoother (and zero after the pulse) in the Born-Oppenheimer case. The Fourier transform of these low-amplitude, smooth curves (or, more precisely, their acceleration form $d^2\langle z\rangle/dt^2$) must lead to smaller intensities, in particular of the higher-order harmonics. In other words and as already stated, the nuclear motion along R has an influence on $\langle z\rangle$; as a consequence, the power spectra are indirectly affected. Another, less striking difference between non-Born-Oppenheimer and Born-Oppenheimer spectra is that the sharp resonances mentioned earlier occur at different positions.

Nuclear motion not only affects HHG emitted light indirectly through its influence on $\langle z\rangle$ (or $d^2\langle z\rangle/dt^2$), it also gives, for $pd\mu$ at least, a *direct* contribution to the HHG signal through $A_R(\omega)$ as will be argued shortly. Power spectra $A_R(\omega)$ of $pp\mu$ and $pd\mu$, calculated in the acceleration form, are presented in Figs. 9(a) and 9(b), respectively.

It is seen from Fig. 9 that, similar to the power spectra $A_z(\omega)$ related to muonic motion along z as presented in Figs. 6 and 7, the power spectrum $A_R(\omega)$ of the homonuclear $pp\mu$ ion contains only odd harmonics [Fig. 9(a)], while in the case of heteronuclear $pd\mu$, it contains both odd and even harmonics [Fig. 9(b)]. This can be explained along similar lines as above. Specifically in the case of nuclear motion under consideration, we can invoke the concept of inversion symmetry of nuclear motion with respect to the center of nuclear mass. Indeed, while in the homonuclear $pp\mu$ ion, two protons are always at the same distances from their center of mass, performing a "symmetric" motion; this symmetry is broken in the heteronuclear $pd\mu$ ion which results in the appearance of even harmonics in the $A_R(\omega)$ spectrum of $pd\mu$.

It is also seen from Fig. 9 that rather high-order harmonics of nuclear motion can be efficiently excited in both $pp\mu$ and $pd\mu$. The strongest harmonic in the $A_R(\omega)$ spectrum of $pp\mu$ [Fig. 9(a)] corresponds to the harmonic order $N_R^{pp\mu} = 23$ and the photon energy of $\hbar\omega = 1.357 \times 10^3$ eV. The strongest harmonic in the $A_R(\omega)$ spectrum of $pd\mu$ [Fig. 9(b)] corresponds to $N_R^{pp\mu} = 15$ and the photon energy of $\hbar\omega = 885$ eV. We see that the maximum excitation of heavier nuclei is lower than that of lighter ones, being in a good agreement with a reasonable relation

$$\frac{N_R^{pp\mu}}{N_R^{pd\mu}} \approx \frac{m_n^{pd\mu}}{m_n^{pp\mu}}, \tag{11}$$

where N_R is the number of the strongest harmonic and m_n stands for the nuclear reduced mass. On the other hand, since

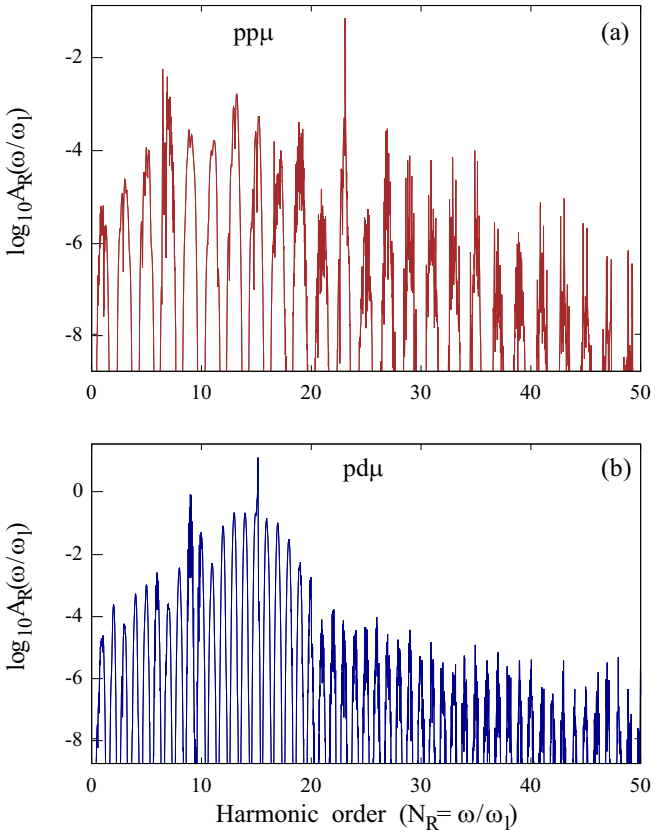

FIG. 9. Power spectra $A_R(\omega)$ generated in $pp\mu$ (a) and $pd\mu$ (b) due to the nuclear motion.

the nuclear motion in the heteronuclear $pd\mu$ ion is excited by the laser pulse directly, the average level of vibrational excitation of $pd\mu$ is substantially higher than that of $pp\mu$, as clearly seen from the comparison of the two $\langle R\rangle$ curves in Fig. 5(b). Obviously, this translates into a higher average intensity of the HHG signals for $pd\mu$ compared to $pp\mu$, at least in the frequency range shown in Fig. 9.

For $pd\mu$, we may quantify the direct nuclear (R) contribution to a measurable, muonic HHG spectrum (polarized along z), in comparison to the purely muonic contribution. Namely, considering that the dipole operator of $pd\mu$ is $\hat{d}_z = bz + cR$ according to Eq. (1), now with factors $b = -e1.0362$ and $c = -e0.3331$, we can compute a HHG signal, polarized along z, in the dipole acceleration form as [18]

$$I_{\rm HHG}^{\rm A}(\omega) \propto \left| \int_0^{t_f} e^{-i\omega t} \frac{d^2}{dt^2} \langle \Psi(t)|bz + cR|\Psi(t)\rangle dt \right|^2. \tag{12}$$

Similarly, we can alternatively compute it in the dipole length form as

$$I_{\rm HHG}^{\rm L}(\omega) \propto \left| \int_0^{t_f} e^{-i\omega t} \langle \Psi(t)|bz + cR|\Psi(t)\rangle dt \right|^2. \tag{13}$$

Now, the direct contribution of nuclear motion to the muonic HHG spectrum, related indirectly to the power spectrum $A_R(\omega)$, can be estimated by simply neglecting the R term in Eq. (12) [assuming that $d^2\langle\Psi(t)|R|\Psi(t)\rangle/dt^2 = 0$], or, in Eq. (13), to fix R to the "fixed R" value of $pd\mu$, which we used for previous Born-Oppenheimer calculations. In both cases, the

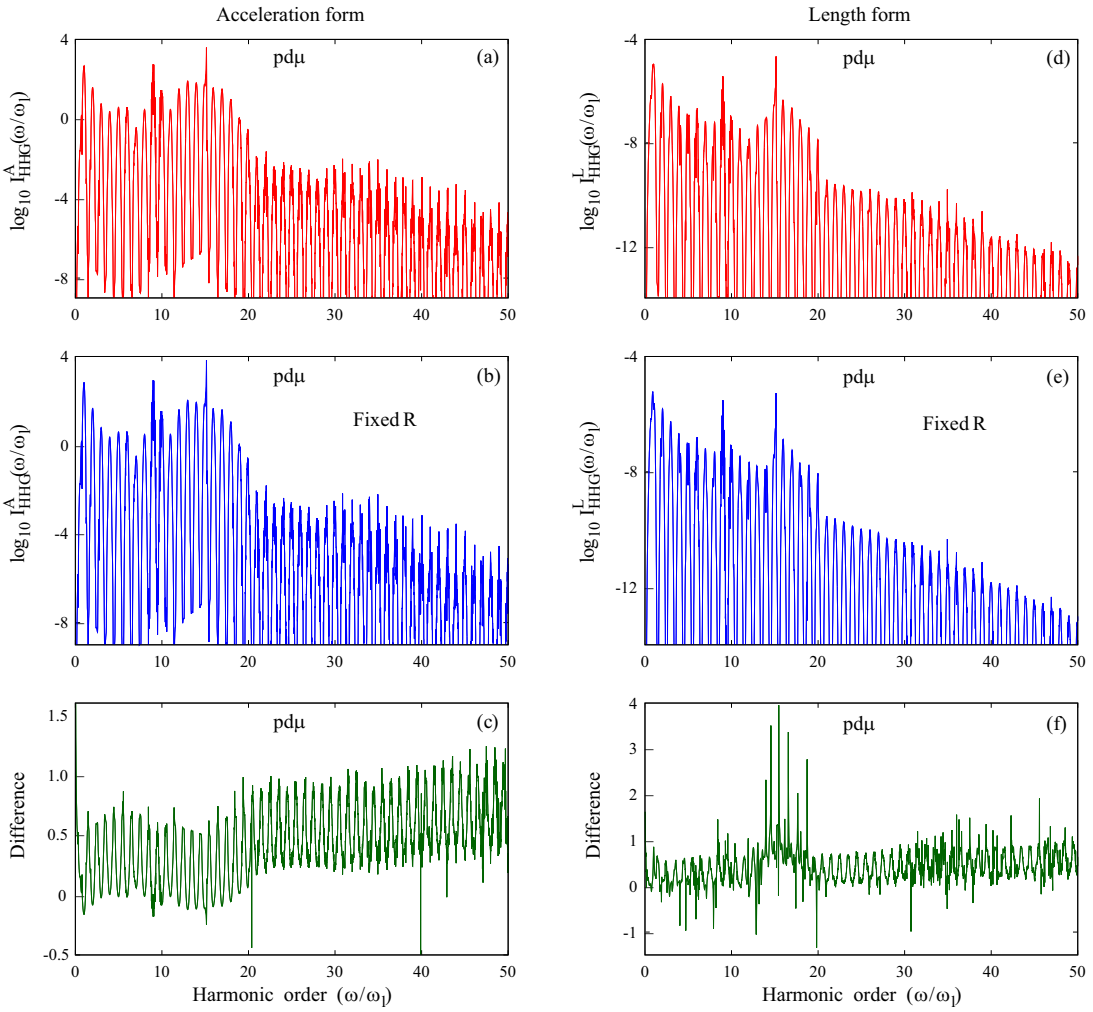

FIG. 10. Comparison of HHG signals in the dipole acceleration form (left panels) and dipole length form (right panels). Panels (a) and (d) give the HHG signals $I^{A}_{\mathrm{HHG}}(\omega)$ and $I^{L}_{\mathrm{HHG}}(\omega)$ obtained from Eqs. (12) and (13), respectively (on a logarithmic scale). Panels (b) and (e) give these signals with the direct contribution from nuclear motion removed ("fixed R"). Panels (c) and (f) show the differences $\Delta = \log_{10} I_{\mathrm{HHG}} - \log_{10} I_{\mathrm{HHG}}$ (fixed R) between the HHG signals with and without the R term.

indirect effect of nuclear motion on dipole expectation values is still included, but the direct contribution of the moving nuclei isn't.

In Figs. 10(a) and 10(d), we show the HHG signals $I^{\mathrm{A}}_{\mathrm{HHG}}(\omega)$ and $I^{\mathrm{L}}_{\mathrm{HHG}}(\omega)$, respectively, obtained from Eqs. (12) and (13) (when setting proportionality constants = 1 and giving intensities in atomic units). In Figs. 10(b) and 10(e), the corresponding spectra are shown when the R terms were neglected or set constant (called fixed R for both, not to be confused with a full Born-Oppenheimer approximation now). Note that in this case the HHG intensity in acceleration form is, apart from the prefactor $b^2 = 1.0737$, the same as $A_z(\omega)$ of $pd\mu$ in Fig. 7(c). We observe the following. (i) At first glance, apart from the different scale, the HHG spectra obtained from the dipole acceleration or the dipole length forms are qualitatively similar, in particular up to $\omega/\omega_l \simeq 20$. (ii) Also the direct contribution of nuclei to the dipole (acceleration) seems small, because the respective fixed R HHG signals with the R term removed or set constant are quite close to those where this was not the case. However, taking the difference between the HHG signals with and without the (constant) R term, i.e., $\Delta I_{\mathrm{HHG}} = I_{\mathrm{HHG}} - I_{\mathrm{HHG}}(R \text{ fixed})$, reveals differences between the two as shown in Figs. 10(c) and 10(e), respectively. Referring to the acceleration form, for example [Fig. 10(c)], closer inspection shows that up to the 20th harmonic intensities themselves (the intensity at integer ω/ω_l values) is hardly affected, and the biggest changes are between the harmonics, at $\omega/\omega_l \simeq 0.5, 1.5, 2.5, \ldots$. For $\omega/\omega_l > 20$, on the other hand, the intensities of the entire fixed R spectra are reduced, resulting in $\Delta I > 0$. Similar, but less clear, trends are observed for HHG signals computed in the dipole length form.

In summary, from comparison of Figs. 7 and 8 we saw that nuclear motion has some effect on muonic power spectra $A_z(\omega)$, for example, which in turn will affect measurable HHG spectra indirectly. From Fig. 9 we note that also clear oscillations exist in power spectra of nuclear motion, $A_R(\omega)$, which, as can be seen from Fig. 10, will translate also into a small direct contribution to measurable, muonic HHG spectra.

Returning to power spectra, an interesting further observation that can be made from the comparison of spectra of $pd\mu$ shown in Figs. 7(c), 7(d), and 9(b) is as follows. In all the three aforementioned power spectra, the 15th harmonic

has a very sharp maximum exactly at $\omega = 15.149\omega_l$, i.e., at $\omega = 32.846$ a.u. ($\hbar\omega \simeq 894$ eV). On the one hand, it was just shown above that the frequency corresponding to this sharp maximum represents characteristic frequencies $\omega_z^{\rm osc}$ and $\omega_\rho^{\rm osc}$ of muonic z and ρ oscillations. On the other hand, it can be found from a detailed analysis of the data presented in Fig. 5(b) for the time-dependent expectation value $\langle R\rangle$ of $pd\mu$ that the same frequency corresponds to the characteristic frequency $\omega_R^{\rm osc}$ of nuclear vibrations. We can conclude, therefore, that the heteronuclear $pd\mu$ ion possesses a unique characteristic frequency $\omega_{\rm osc}^{pd\mu}$ that represents both characteristic frequencies of muonic z and ρ oscillations and the characteristic frequency of nuclear vibrations, which manifest themselves by very sharp maxima in the corresponding power spectra. In contrast, the homonuclear $pp\mu$ ion does not possess such a unique characteristic frequency.

VI. CONCLUSIONS

In the present work, the non-Born-Oppenheimer quantum dynamics of muonic molecular ions $pp\mu$ and $pd\mu$ excited by a superintense, short five-cycle laser pulse linearly polarized along the molecular axis has been studied by the numerical solution of the time-dependent Schrödinger equation within a three-dimensional model, including the internuclear distance R and muon coordinates z and ρ, which have been treated explicitly. Several simulations have been also performed at a fixed internuclear distance R, such as to check the applicability of the Born-Oppenheimer approximation.

The main results obtained in the work can be summarized as follows.

(i) During the laser pulse, the heavy muon approximately follows the laser field out of phase—the expectation value $\langle z\rangle$ of the optically active z degree of freedom decreases when the strength of the applied laser field increases.

During the free evolution after the end of the pulse, expectation values $\langle z\rangle$, $\langle\rho\rangle$, and $\langle R\rangle$ demonstrate rather complicated free oscillations. The post-laser-pulse oscillations of $\langle z\rangle$ and $\langle R\rangle$ occur out of phase and appear as shaped echo pulses in the case of $pd\mu$.

The post-laser-pulse oscillations of $\langle z\rangle$ and $\langle\rho\rangle$ do not occur if the internuclear distance R is fixed, implying that the appearance of post-laser-pulse muonic oscillations is a purely non-Born-Oppenheimer phenomenon.

(ii) Power spectra related to the nuclear motion and those related to muonic motion along both optically active z and optically passive ρ degrees of freedom have been calculated in the acceleration form.

It has been found that the power spectrum of muonic z oscillations in $pp\mu$ contains only odd harmonics, as anticipated by the concept of inversion symmetry of muonic motion in the homonuclear $pp\mu$ ion (on the analogy with inversion symmetry of electronic motion in the homonuclear H_2 molecule [18]). In contrast, the power spectrum of muonic ρ oscillations in $pp\mu$ contains only even harmonics, which can be explained by the effect of frequency doubling of optically passive ρ oscillations induced by the laser driven z oscillations due to the wave properties of the muon [8].

The power spectrum of muonic z oscillations in $pd\mu$ contains both odd and even harmonics, which is explained by the fact that inversion symmetry of muonic motion in the heteronuclear $pd\mu$ ion is broken. The power spectrum of muonic ρ oscillations in $pd\mu$ also contains both even and odd harmonics, which is explained by the effect of frequency doubling of ρ oscillations, on the one hand, and by the combined effects of the frequency-doubled even harmonics of ρ oscillations and the first harmonic of ρ oscillations that appears already during the laser pulse due to the wave properties of the muon, on the other hand.

Similar to power spectra of muonic z oscillations in $pp\mu$ and $pd\mu$, the power spectrum related to nuclear motion in $pp\mu$ contains only odd harmonics, while that of the heteronuclear $pd\mu$ ion contains both even and odd harmonics. This is explained on the basis of the concept of inversion symmetry of nuclear motion in $pp\mu$ and $pd\mu$, which is invoked in our work, on the analogy of inversion symmetry of electronic and muonic motion in the homonuclear and heteronuclear systems.

Finally, it is found that the heteronuclear $pd\mu$ ion possesses a unique characteristic frequency that represents two characteristic frequencies of muonic oscillations and the characteristic frequency of nuclear vibrations, which manifest themselves by very sharp maxima in the corresponding power spectra of $pd\mu$. The homonuclear $pp\mu$ ion does not possess such a unique characteristic frequency.

(iii) Power spectra and HHG spectra are influenced by nuclear motion. Both for $pp\mu$ and $pd\mu$ the nuclear motion affects muonic motion, which has an indirect influence on power and HHG spectra. In the case of $pd\mu$, also a non-negligible direct contribution of nuclear motion to the HHG spectrum can be expected.

In general, muonic molecular ions driven by intense, short laser pulses offer not only a way to enhanced nuclear fusion [8,9], they could also serve as fascinating microlabs for creating very high-energy harmonics and for evaluating basic concepts of molecular quantum mechanics, such as the Born-Oppenheimer approximation.

ACKNOWLEDGMENT

We acknowledge fruitful discussions with A. D. Bandrauk (Sherbrooke).

APPENDIX A: NUMERICAL METHODS TO SOLVE THE 3D SCHRÖDINGER EQUATION

In the very first theoretical works [20,21] where the explicit treatment of the electron motion with the time-dependent Schrödinger equation was employed, single-electron model atoms excited by linearly polarized laser fields were numerically investigated. Subsequently, more complicated problems, such as the 3D hydrogen atom excited by a strong elliptically polarized laser field [22], were addressed. The non-Born-Oppenheimer quantum dynamics of molecules in very strong laser fields introduced a challenge to numerical techniques due to the appearance of a new degree of freedom, the internuclear distance R, which had to be treated explicitly. In the first works along these lines [23,24], the laser-driven quantum dynamics of simple molecular ion H_2^+ was studied. Subsequently, the problem of laser-enhanced fusion in muonic molecular ions $dd\mu$ and $dt\mu$ was also addressed [11–13].

Numerical techniques used to solve the 3D equation of motion (3) have been described in detail in our previous works [13,14]. In particular, muonic motion along the z and ρ degrees of freedom has been treated by making use of the polynomial expansion of the wave function over the Hermite $H_n(z)$ and the Laguerre $L_m(\rho)$ polynomials, respectively, and subsequent integration on the corresponding quadrature points for calculation of the expectation values.

Specifically, the z grid is defined by the quadrature points of the Hermite polynomials and is not equidistant. Our z grid has 200 points and ranges from $z = -1.2092$ a.u. to +1.2093 a.u., where $z = 0$ is not a quadrature point. The size of the z grid was chosen such as to be larger than the maximum excursion of the muon along the z axis, $\alpha = \mathcal{E}_0/(M_\mu \omega_l^2)$. With the electric-field amplitude $\mathcal{E}_0 = 1 \times 10^3$ a.u., the laser carrier frequency $\hbar\omega_l = 2.1682$ a.u., used in the present work, and the muon mass $M_\mu = 206.768$ a.u., one gets $\alpha = 1.029$ a.u.. The choice of the z grid was based on this value and the size of the ρ grid has been chosen accordingly. Specifically, the 3D wave packet was damped with the imaginary smooth optical potentials, adapted from [25], at $z < -1.2$ a.u., at $z > 1.2$ a.u., and at $\rho > 1.15$ a.u. for the muonic motion and at $R > 1.1$ a.u. for the nuclear motion.

The ρ grid is also nonequidistant and defined by the quadrature points of the Laguerre polynomials on a 100-point grid.

Nuclear motion has been treated with the split-operator method and FFT (fast Fourier transform) on the equidistant grid for the R degree of freedom, using a time step of 3.505×10^{-6} fs. The R grid is equidistant with 1024 points and a spacing of 0.00125 a.u., the last point being $R = 1.27875$ a.u. The first point is defined within the nuclear drop model as $R(1) = 2(r_d + r_p)/3$ for $pd\mu$ and $4r_p/3$ for $pp\mu$, respectively, giving $R(1) = 0.22049 \times 10^{-4}$ a.u. for $pp\mu$, for example.

Within the nuclear drop model used in the present work, corrections to the ground-state energies of $pp\mu$ and $pd\mu$ caused by nuclear size effects are accounted for automatically. Other relativistic and quantum electrodynamical corrections, see e.g. [26,27], have not been taken into account in the present work since they are very small compared to the ground-state energies. Indeed, playing the leading role vacuum-polarization corrections to the ground-state energies are really small: -0.295 eV (-0.0108 a.u.) and -0.305 eV (-0.0112 a.u.) for $pp\mu$ and $pd\mu$, respectively [26]. In both cases, aforementioned corrections are less than 0.01% of the ground-state energies and, in fact, do not influence neither the laser-driven dynamics nor the power and HHG spectra presented above.

Finally, in order to control the accuracy of our simulations, we used the time-dependent consistency check,

$$\mathcal{N}(t) + D(t) + I_{z(+)}(t) + I_{z(-)}(t) + I_\rho(t) = 1, \qquad \text{(A1)}$$

where $\mathcal{N}(t)$ is the norm remaining on the 3D grid between the absorbing boundaries, $D(t)$ is the dissociation probability, $I_{z(\pm)}(t)$ are ionization probabilities in the positive and in the negative direction of the z axis, and $I_\rho(t)$ is the ionization probability from the outer end of the ρ axis. The consistency check of Eq. (A1) was fulfilled in out simulations to better than 0.01% accuracy.

APPENDIX B: ESTIMATE OF THE HHG CUTOFF ENERGY BASED ON THE THREE-STEP MODEL

The HHG cutoff energy $\hbar\omega_{\rm cut}$ according to the classical three-step model [19] is given by Eq. (10). Let us estimate very roughly for the muonic systems the latter by replacing M_e by M_μ and taking for IP the *vertical* ionization potential, given by $E_{\rm bind} + {\rm IP(atom)} + 1/R_0$. Here, $E_{\rm bind}$ is the binding energy with respect to dissociation as defined earlier, IP(atom) the atomic ionization energy of $p\mu$ or $d\mu$, respectively, and $1/R_0$ the nuclear repulsion in pp (or pd) at the equilibrium distance of $pp\mu$ (or $pd\mu$), for which we take $R_0 = 0.0097$ a.u. of above. We then get IP $\simeq 205.5$ a.u. (for $pp\mu$) and IP $\simeq 209.4$ a.u. (for $pd\mu$), and for $U_p \simeq 257.5$ a.u. This gives, for $pp\mu$, an expected cutoff energy of $\hbar\omega_{\rm cut} \simeq 1021.8$ a.u., corresponding to a highest-order harmonic of $N_{\rm cut} = \omega_{\rm cut}/\omega_l = \simeq 471$. A similar estimate for $pd\mu$ gives $N_{\rm cut} \simeq 473$. Of course, in a more elaborate treatment nuclear motion should be taken into account, which would reduce IP substantially. Also, reduced (rather than pure) muon masses should be used for the ponderomotive energy U_p [3], which would lead to different U_p for $pp\mu$ and $pd\mu$. Finally, quantum-mechanical effects and effects due to the pulsed (rather than continuous wave) nature of the exciting laser field may be of importance. Still, the main conclusions formulated in the main text should hold, that (i) the "true" cutoff regions of HHG spectra of $pp\mu$ and $pd\mu$ are not yet reached in Fig. 6 and (ii) some (small) differences are to be expected for the overall shape of HHG spectra of both isotopomers.

[1] A. Shahbaz, C. Müller, T. J. Bürvenich, and C. H. Keitel, Phys. Rev. Lett. **98**, 263901 (2007).

[2] A. Shahbaz, C. Müller, T. J. Bürvenich, and C. H. Keitel, Nucl. Phys. A **821**, 106 (2009).

[3] A. Shahbaz, T. J. Bürvenich, and C. Müller, Phys. Rev. A **82**, 013418 (2010).

[4] Y. Xiang, Y. Niu, R. Li, and S. Gong, J. Mod. Opt. **57**, 385 (2010).

[5] Z.-C. Li, S. Cui, and F. He, Act. Phys. Sin. **63**, 073201 (2014).

[6] K. Ishida, K. Nagamine, T. Matsuzaki, and N. Kawamura, J. Phys. G: Nucl. Part. Phys. **29**, 2043 (2003).

[7] K. Nagamine and L. Ponomarev, Nucl. Phys. A **721**, C863 (2003).

[8] A. D. Bandrauk and G. K. Paramonov, Int. J. Mod. Phys. E **23**, 1430014 (2014).

[9] L. I. Ponomarev, Contemp. Phys. **31**, 219 (1990).

[10] A. Carrington, I. R. McNab, and C. A. Montgomerie, J. Phys. B **22**, 3551 (1989).

[11] S. Chelkowski, A. D. Bandrauk, and P. B. Corkum, Laser Phys. **14**, 473 (2004).

[12] S. Chelkowski, A. D. Bandrauk, and P. B. Corkum, Phys. Rev. Lett. **93**, 083602 (2004).

[13] G. K. Paramonov, Chem. Phys. **338**, 329 (2007).

[14] G. K. Paramonov, Chem. Phys. Lett. **411**, 350 (2005).

[15] G. K. Paramonov, O. Kühn, and A. D. Bandrauk, J. Phys. Chem. A **120**, 3175 (2016).

[16] G. K. Paramonov, O. Kühn, and A. D. Bandrauk, Mol. Phys. **115**, 1846 (2017).
[17] P. Salières, P. Antoine, A. de Bohan, and M. Lewenstein, Phys. Rev. Lett. **81**, 5544 (1998).
[18] T. Kreibich, M. Lein, V. Engel, and E. K. U. Gross, Phys. Rev. Lett. **87**, 103901 (2001).
[19] P. Corkum, Phys. Rev. Lett. **71**, 1994 (1993); J. L. Krause, K. J. Schafer, and K. C. Kulander, *ibid.* **68**, 3535 (1992).
[20] K. C. Kulander, Phys. Rev. A **35**, 445 (1987).
[21] J. Javanainen, J. H. Eberly, and Q. Zu, Phys. Rev. A **38**, 3430 (1988).
[22] V. S. Melezhik, Phys. Lett. A **230**, 203 (1997).
[23] S. Chelkowski, T. Zuo, O. Atabek, and A. D. Bandrauk, Phys. Rev. A **52**, 2977 (1995).
[24] I. Kawata, H. Kono, and Y. Fujimura, J. Chem. Phys. **110**, 11152 (1999).
[25] M. Kaluža, J. T. Muckerman, P. Gross, and H. Rabitz, J. Chem. Phys. **100**, 4211 (1994).
[26] V. S. Melezhik and L. I. Ponomarev, Phys. Lett. B **77**, 217 (1978).
[27] D. Bakalov and V. I. Korobov, Hyperfine Interact. **138**, 265 (2001).